Efficient Sub-Gridded FDTD for Three-Dimensional Time-Reversed Electromagnetic Field Shaping

Xiao-Kun Wei, Wei Shao, Xiao Ding, and Bing-Zhong Wang

School of Physics
University of Electronic Science and Technology of China, Chengdu, Sichuan 610054, China
weixiaokun1990@163.com, weishao@uestc.edu.cn, xding@uestc.edu.cn, bzwang@uestc.edu.cn

Abstract ─ Based on the space-time focusing property of the time reversal technique, the electromagnetic field shaping of arbitrary patterns is easily realized by using an efficient sub-gridded finite-difference time-domain (FDTD) method in this paper. It is an electrically large and multiscale problem if the desired shaping field requires high resolution. With the advantage of the sub-gridded scheme, the electromagnetic field shaping region can be locally discretized with dense grids, which is embedded in global coarse grids. Then, the Courant-Friedrich-Levy (CFL) limit can be extended by employing the spatial filtering scheme to filter out the unstable harmonics inside the dense grid region. Thus, the number of total unknowns is largely reduced and a common time step size chosen from the CFL limit of the coarse grid is used throughout the computational domain. Simulation results with two kinds of boundary conditions are provided to demonstrate the availability of the spatially-filtered sub-gridded FDTD method for electromagnetic field shaping.

Index Terms ─ Electromagnetic field shaping, finite-difference time-domain (FDTD) method, sub-gridded scheme, time reversal (TR) technique.

I. INTRODUCTION

The time reversal (TR) technique, which is very promising in controlling electromagnetic waves in complex media due to its space-time focusing property [1]-[4] and super-resolution characteristic [5]-[7], has been widely employed in wireless communications, microwave imaging and detection, medical treatment, and wireless power transformation [8], [9]. Based on the TR technique, the "L"-shaped electromagnetic field was generated through experiment in an aluminum cavity [10], which provides an effective way to physically generate arbitrarily shaped microwave fields inside an interested region. Source reconstruction, realized by using several methods [11]-[14], is very similar to the electromagnetic field shaping. Different from the field shaping, the source reconstruction is to find unknown sources by using the received signals at preselected output locations.

To numerically solve such a time-domain electromagnetic problem, the finite-difference time-domain (FDTD) method is often employed because of its simplicity and versatility [15]. Usually, there are ten to twenty wavelengths along each direction in the computational region of electromagnetic field shaping. If a predefined field pattern requires high spatial resolution, this area is discretized with fine grids. In the FDTD simulation, a maximal size of the time step should be determined by a minimal size of the spatial grid in order to keep numerical stability, according to the Courant-Friedrich-Levy (CFL) condition [15]. Thus, the computational efficiency of FDTD with uniform dense grids is strictly constrained due to the large number of unknowns and a very small time step size.

On the one hand, to reduce the number of total unknowns of an electrically large structure, a sub-gridded scheme in which local dense grids are located inside global coarse grids is a good fit [16]. On the other hand, to extend the CFL limit imposed by the minimal grid size of a computational domain involving multiscale grid division, the spatial filtering scheme can be used to filter out the unstable harmonics inside the sub-gridded region [17], [18]. In this paper, combined with two procedures of the TR technique, an efficient spatially-filtered sub-gridded FDTD method is employed to implement the electromagnetic field shaping in three-dimensional (3D) space with two different boundary conditions. According to the CFL limit of the coarse grid, a common time step size can be chosen for the whole computational domain in a stable fashion. In the numerical experiments, "L"-shaped and "E"-shaped microwave fields are generated within a perfectly electric conductor (PEC) cavity, as presented in [10], to demonstrate the availability of the proposed method. Furthermore, these two desired patterns are generated in free space truncated by the perfectly matched layer (PML) [19]. For the free space case, more TR antenna elements are needed to have a high-quality shaped microwave field.

The rest of this paper is organized as follows. In Section II, the numerical implementation for generating

Submitted On: June 11, 2018
Accepted On: August 11, 2018

an arbitrarily shaped electromagnetic field is given. Section III verifies the accuracy and efficiency of the spatially-filtered sub-gridded FDTD method and shows the numerical results of generating various field patterns. The conclusion is presented in Section IV.

II. THEORIES AND FORMULATIONS

Based on the TR technique, the microwave field is generated by locating a shaping antenna array inside the electromagnetic shaping region and by placing a TR antenna array outside, as shown in Fig. 1.

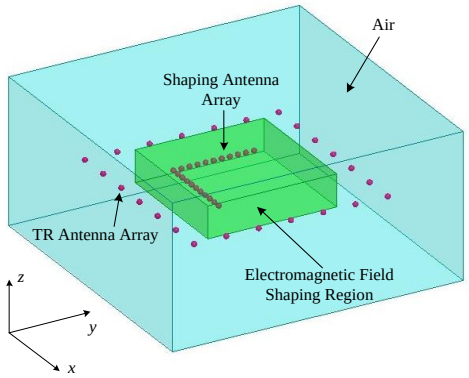

Fig. 1. Computational domain of generating a predefined electromagnetic field based on the TR technique.

With reference to [20], the time-reversed electric field vector can be rewritten in frequency domain as:

$$\boldsymbol{E}^{\mathrm{TR}}(\boldsymbol{r},\boldsymbol{r}_s;\omega)=-\frac{\omega\mu}{\lambda}\left\{\left(\overline{\overline{I}}+\frac{\nabla\nabla}{k^2}\right)\left(\frac{\sin k|\boldsymbol{r}-\boldsymbol{r}_s|}{k|\boldsymbol{r}-\boldsymbol{r}_s|}\right)\right\}\boldsymbol{i}^*(\omega), \tag{1}$$

which indicates that $\boldsymbol{E}^{\mathrm{TR}}(\boldsymbol{r}, \boldsymbol{r}_s; \omega)$ will be maximized at the original source point $\boldsymbol{r}_s$. The time-domain time-reversed electric field vector can also be given by inverse Fourier transform as:

$$\boldsymbol{E}^{\mathrm{TR}}(\boldsymbol{r},\boldsymbol{r}_s;t)=\mu\frac{\partial}{\partial t}\int_{-\infty}^{+\infty}\left\{\overline{\overline{G}}^{*}(\boldsymbol{r},\boldsymbol{r}_s)-\overline{\overline{G}}(\boldsymbol{r},\boldsymbol{r}_s)\right\}\boldsymbol{i}^*(\omega)\,\mathrm{e}^{\mathrm{j}\omega t}\mathrm{d}\omega, \tag{2}$$

which means that the time-reversed electric field vectors $\boldsymbol{E}^*(\boldsymbol{r}, \boldsymbol{r}_s)$ will simultaneously arrive at $\boldsymbol{r}_s$ and accumulated with each other, wherever the $\boldsymbol{E}^*(\boldsymbol{r}, \boldsymbol{r}_s)$ is located. The combination of (1) and (2) demonstrates the space-time focusing property of the time-reversed electromagnetic waves. Based on this property, we can closely place several shaping antenna elements to generate a smooth field of the desired shape.

To numerically realize the electromagnetic field shaping with an arbitrary microwave pattern, an efficient sub-gridded FDTD with extended CFL limit is a good choice. Since the spatial filtering scheme is employed to filter out the unstable harmonics of the dense grid, the 3D CFL limit inside the sub-gridded region can be extended and rewritten as:

$$\Delta t \le \Delta t_{\mathrm{CFL}} \times CE, \tag{3}$$

where Δt_{CFL} is the conventional CFL limit of the dense grid, and *CE* is a CFL extension factor that is defined as:

$$CE=\frac{1}{\sin\dfrac{k_{\max}\Delta}{2\sqrt{3}}}, \tag{4}$$

where Δ is the spatial grid size, $k_{\max}$ is the maximal value of the numerical wavenumbers determined by a desired *CE* factor. To implement the spatial filtering scheme, three additional stages are incorporated into the FDTD time-stepping algorithm. Firstly, the magnetic field components inside the sub-gridded region are transformed into frequency domain by Fourier transform. Secondly, a spherical low-pass spatial filter is defined as:

$$\overline{\boldsymbol{F}}(\boldsymbol{k})=\begin{cases}1, & \text{for } \sqrt{k_x^2+k_y^2+k_z^2}\le k_{\max}\\ 0, & \text{otherwise}\end{cases}, \tag{5}$$

which is applied to the frequency-domain magnetic field components inside the sub-gridded region. Thirdly, the filtered magnetic field components are transformed back to the space domain by inverse Fourier transform. Thus, a common time step size calculated from the CFL limit of the coarse grid can be used throughout the computational region, and no interpolation and extrapolation is needed to synchronize coarse and dense grids in temporal domain.

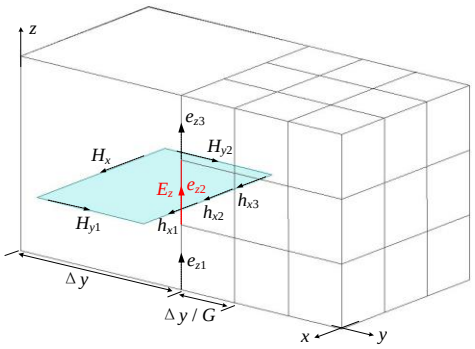

Fig. 2. Electromagnetic field component arrangement at the coarse-dense grid interface for a mesh refinement ratio of three.

In spatial domain, the tangential electric field components are located on the interfaces of the coarse and dense grids. Here, the grid refinement ratio *G* is chosen as 3. Then, the data are exchanged via contour integrals of weighted coarse and dense fields, as shown in Fig. 2. Field components in the coarse grid are denoted by capital letters and those in the dense grid are shown with the lower case letters. To illustrate the data-exchanging scheme on the interfaces, the electric field component of E_z is taken as an example.

On the interfaces, the update equation of E_z, constructed from the integral form of the Maxwell's equations, is given as:

$$E_z^{n+1}\Big|_{i,j,k+\frac{1}{2}} = E_z^{n}\Big|_{i,j,k+\frac{1}{2}} + \frac{\Delta t}{\varepsilon_0 \Delta x}\left(H_y^{n+\frac{1}{2}}\Big|_{i+\frac{1}{2},j,k+\frac{1}{2}} - H_y^{n+\frac{1}{2}}\Big|_{i-\frac{1}{2},j,k+\frac{1}{2}} \right) - \frac{\Delta t}{\varepsilon_0 \Delta y}\left(H_x^{n+\frac{1}{2}}\Big|_{i,j+\frac{1}{2},k+\frac{1}{2}} - H_x^{n+\frac{1}{2}}\Big|_{i,j-\frac{1}{2},k+\frac{1}{2}} \right). \quad (6)$$

As revealed in Fig. 2, the effective area of the contour on the interface is changed. Therefore, the formulation to update E_z is a modified form of (6), which is:

$$E_z^{n+1} = E_z^{n} + \frac{\Delta t}{\varepsilon_0 \Delta x}\left(H_{y1}^{n+\frac{1}{2}} - H_{y2}^{n+\frac{1}{2}} \right) - \frac{\Delta t}{\varepsilon_0 \Delta y \dfrac{G+1}{2G}}\left(\sum_{i=1}^{G} \frac{1}{G} h_{xi}^{n+\frac{1}{2}} - H_x^{n+\frac{1}{2}} \right), \quad (7)$$

and e_z is directly calculated from E_z by:

$$e_{zi}(i = 1, 2, \cdots, G) = E_z. \quad (8)$$

Once the electric field components e_z on the interfaces are obtained from (8), both electric and magnetic field components can be updated with a large time step size inside the sub-gridded region.

The flowchart in which the spatially-filtered sub-gridded FDTD method and the TR technique are combined to generate a desired electromagnetic field is shown in Fig. 3. The TR process defines the original excitation and boundary condition of a predefined electromagnetic field shaping scenario and sends those initial parameters to the spatially-filtered sub-gridded FDTD simulation. Then, the spatially-filtered sub-gridded FDTD calculates wave propagation and returns the time-domain waveforms back to the TR technique. Finally, the desired microwave field can be achieved.

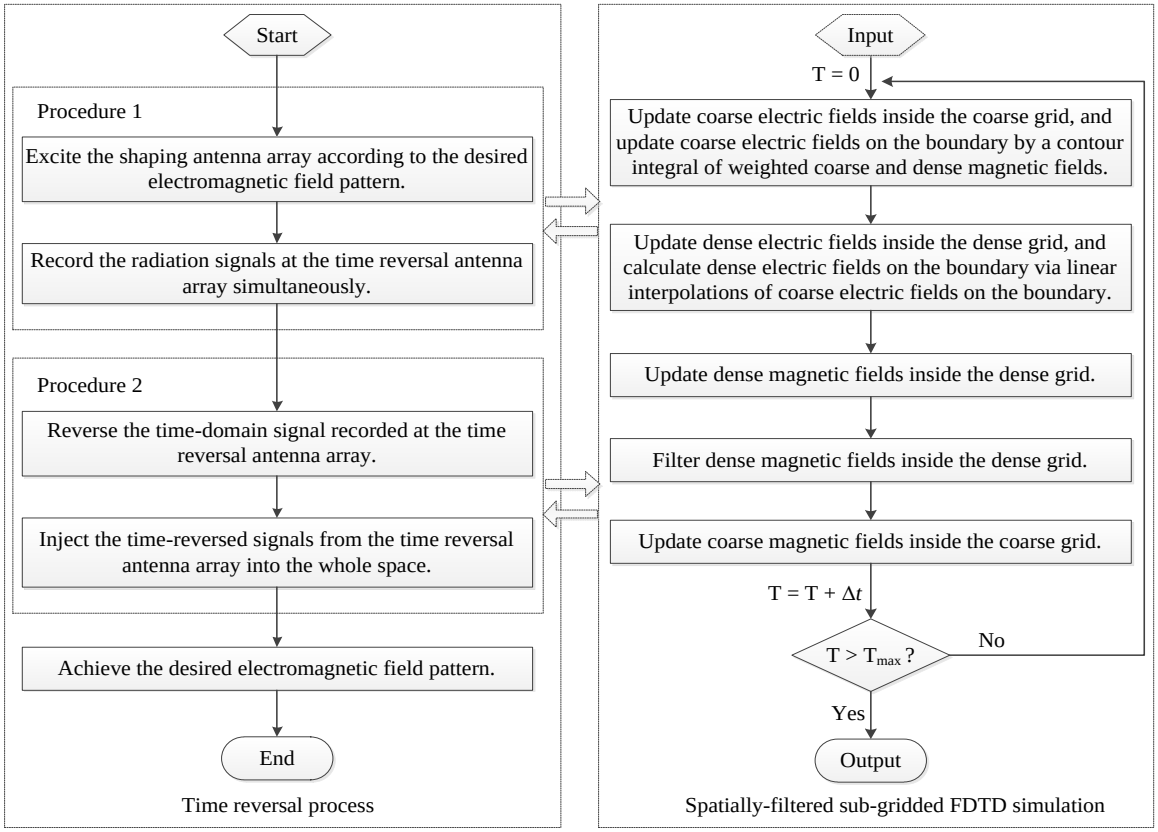

Fig. 3. Flowchart of the numerical implementation to generate an arbitrarily shaped electromagnetic field.

III. NUMERICAL RESULTS

Numerical examples of the time-reversed electromagnetic field shaping with different boundary conditions are provided in this section, demonstrating the accuracy and efficiency of the spatially-filtered sub-gridded FDTD method for solving multiscale and electrically large TR problems. Here, all calculations are performed on an Intel(R) Core(TM) i7-4790×8 CPU @ 3.60 GHz machine with 16 GB RAM.

A. Numerical validation

To begin with, a PEC cavity, whose size is 6 cm ×

9 cm × 6 cm along the *x*-, *y*- and *z*-directions, respectively, is calculated by the FDTD, sub-gridded FDTD and spatially-filtered sub-gridded FDTD methods. The cubic dense grids with Δ_{dense} = 1 mm are used in the FDTD simulation. For the two sub-gridded FDTD methods, a sub-gridded region locally discretized by cubic dense grids is embedded in the global region divided into cubic coarse grids with Δ_{coarse} = 3 mm. The time step size for both FDTD and sub-gridded FDTD is determined by the CFL limit of the dense grid, and 3000 time-marching steps are needed to obtain the time-domain waveforms. For the spatially-filtered sub-gridded FDTD, a time step size defined by the CFL limit of the coarse grid can be employed throughout the computational domain, enabled by the spatial filtering, and only 1000 time-marching steps are required to cover the same time interval.

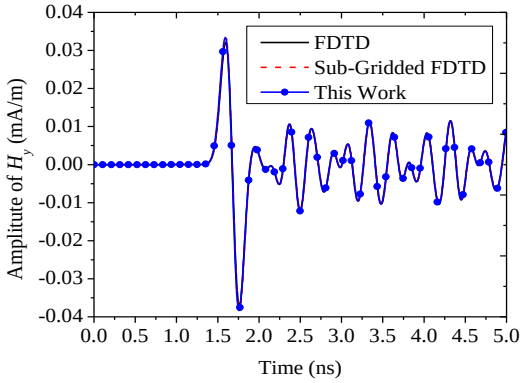

Fig. 4. Time-domain waveforms of the PEC cavity calculated from the three methods.

Table 1: Comparison of execution time and memory requirement for the three methods

Methods	CPU Time (s)	Memory (MB)
FDTD	756.94	189.37
Sub-gridded FDTD	71.09	25.34
This work	46.56	26.68

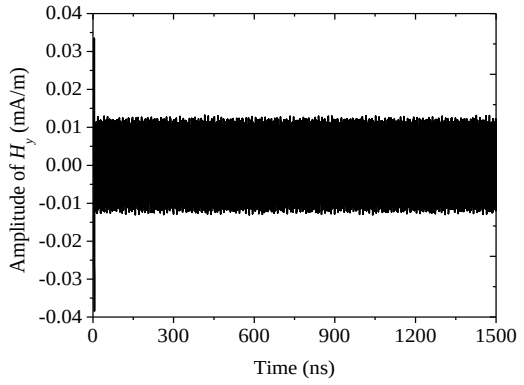

Fig. 5. Stability verification of the spatially-filtered sub-gridded FDTD method by running 300000 time-marching steps.

The excitation is a Gaussian pulse where the maximal frequency is 900 MHz. The time-domain waveforms in Fig. 4 show the excellent agreement among the three methods and demonstrate the numerical accuracy of the spatially-filtered sub-gridded FDTD. The execution time and memory requirement of the three methods are presented in Table 1, indicating that the CPU time of the proposed method is largely reduced compared with the other two methods. Furthermore, the late time stability of the spatially-filtered sub-gridded FDTD is also verified by running 300000 time-marching steps, as shown in Fig. 5.

B. PEC boundary condition

The electromagnetic field shaping within a metal cavity implemented by PEC boundary condition is considered here, as shown in Fig. 1. The maximal frequency of a Gaussian pulse which is employed as the excitation is 2.45 GHz, and the corresponding wavelength λ is 122.45 mm in free space. The whole computational domain is 2.16 m × 2.16 m × 1.08 m and it is divided into cubic coarse grids with Δ_{coarse} = 9 mm. A sub-gridded region with spatial size of 0.48 m × 0.48 m × 0.12 m, which is located in the center of the cavity, is divided into cubic dense grids with Δ_{dense} = 3 mm. As before, the time step size of the sub-gridded FDTD is defined by the CFL limit of the dense grid and 90000 time-marching steps are required. However, a time step size assigned by the CFL limit of the coarse grid can be used in the spatially-filtered sub-gridded FDTD, and only 30000 time-marching steps are needed. The FDTD simulation with a uniform dense grid requires too large memory and execution time, and it is omitted.

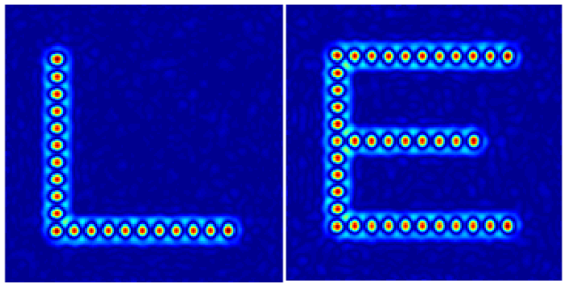

Fig. 6. Shaped electromagnetic field patterns calculated by the spatially-filtered sub-gridded FDTD within a metal cavity: (a) "L"-shaped field, and (b) "E"-shaped field.

Table 2: Computational effort for the PEC case

Methods	CPU Time (h)	Memory (GB)
Sub-gridded FDTD	54.56	2.78
This work	25.42	3.03

In the TR antenna array, there are 48 elements and the distance between two elements is 0.12 m. The shaping

antenna array is ranged according to the desired pattern of the electromagnetic field. Here, both "L"-shaped and "E"-shaped fields are considered, and the distance between two shaping antennas is 0.03 m. Figure 6 shows the results of two desired field patterns calculated by the spatially-filtered sub-gridded FDTD method with extended CFL limit of the dense grid. The execution time and memory requirement of the two methods are presented in Table 2, revealing the reduced CPU time enabled by the spatial filtering scheme in cost of slightly larger memory requirement.

C. PML boundary condition

In this part, the electromagnetic field shaping in the free space implemented by 10-cell-thick PML is also considered. The time-marching steps for the sub-gridded FDTD and spatially-filtered sub-gridded FDTD are 9000 and 3000, respectively. The set-up of this problem is same as that of the PEC case. The results of "L"-shaped and "E"-shaped field patterns are presented in Fig. 7.

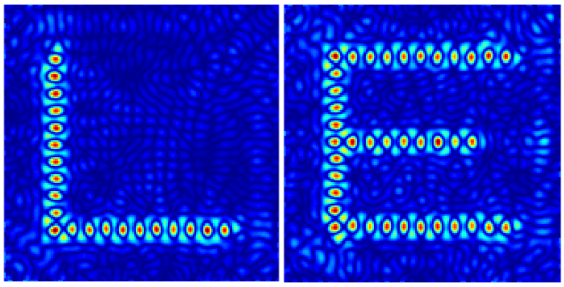

(a) (b)

Fig. 7. Shaped electromagnetic field patterns in free space calculated by the spatially-filtered sub-gridded FDTD with 48 elements in the TR antenna array: (a) "L"-shaped field, and (b) "E"-shaped field.

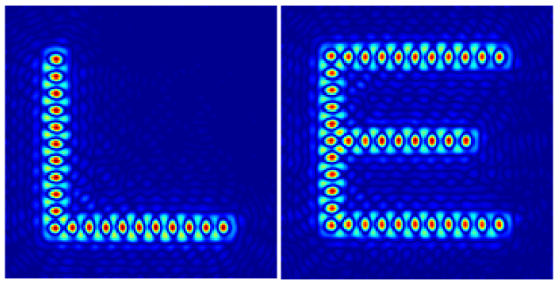

(a) (b)

Fig. 8. Shaped electromagnetic field patterns in free space calculated by the spatially-filtered sub-gridded FDTD with 192 elements in the TR antenna array: (a) "L"-shaped field, and (b) "E"-shaped field.

When the TR array consists of 192 elements, the shaped fields are revealed in Fig. 8. Table 3 also gives the computational efforts of the two methods in free space and demonstrates the efficiency of the spatially-filtered sub-gridded FDTD.

Table 3: Computational effort for the PML case

Methods	CPU Time (h)	Memory (GB)
Sub-gridded FDTD	24.61	11.61
This work	8.82	12.46

D. Discussion

To begin with, due to the multipath propagating property of the metal cavity, the time-reversed electromagnetic field can be focused on a predefined pattern with a relatively large number of time-marching steps. Furthermore, the electromagnetic waves are multi-reflected inside the closed region without attenuation, and thus 48 elements in the TR antenna array are enough to capture required signals. However, for the free space case, since the electromagnetic field is absorbed and attenuated in the PML region, more elements in the TR antenna array are required to obtain a high quality shaped electric field. Fewer time-marching steps are needed in this case because of the PML truncation. It can be pointed out that the generated microwave fields in Figs. 6 and 8 have almost the same quality. The other shaped patterns of the electromagnetic field can also be easily achieved in the same way.

IV. CONCLUSION

In this paper, an efficient sub-gridded FDTD method is employed for simulating the electrically large and multiscale TR electromagnetic field shaping of arbitrary microwave patterns, whose electric size is approximately $18\,\lambda \times 18\,\lambda \times 9\,\lambda$. Enabled by the spatial filtering scheme, both the coarse and dense grids are run with a large time step size defined by the CFL limit of the coarse grid, and two patterns of electromagnetic field with both PEC and PML boundary conditions are realized. The simulation results demonstrate that the spatially-filtered sub-gridded FDTD is powerful in solving electrically large TR scenarios with locally fine grid division. In the future work, the codes will be implemented in a parallel manner to further improve the computational efficiency.

ACKNOWLEDGMENT

This work was supported by the National Natural Science Foundation of China under Grant 61471105 and Grant 61331007.

REFERENCES

[1] G. Lerosey, J. de Rosny, A. Tourin, et al., "Time reversal of electromagnetic waves," *Phys. Rev. Lett.*, vol. 92, no. 19, Art. no. 193904, May 2004.

[2] X. Xu, H. Liu, and L. V. Wang, "Time-reversed ultrasonically encoded optical focusing into scattering media," *Nature Photon.*, vol. 5, pp. 154-

157, Mar. 2011.

[3] X. K. Wei, W. Shao, S. B. Shi, Y. F. Cheng, and B. Z. Wang, "An optimized higher order PML in domain decomposition WLP-FDTD method for time reversal analysis," *IEEE Trans. Antennas Propag*., vol. 64, no. 10, pp. 4374-4383, Oct. 2016.

[4] X. K. Wei, W. Shao, H. Ou, and B. Z. Wang, "An efficient higher-order PML in WLP-FDTD method for time reversed wave simulation," *J. Comput. Phys*., vol. 321, no. 9, pp. 1206-1216, Aug. 2016.

[5] J. de Rosny and M. Fink, "Focusing properties of near-field time reversal," *Phys. Rev. A*, vol. 76, no. 6, Art. no. 065801, 2007.

[6] G. Lerosey, J. de Rosny, A. Tourin, and M. Fink, "Focusing beyond the diffraction limit with far-field time reversal," *Science*, vol. 315, no. 5815, pp. 1120-1122, Feb. 2007.

[7] X. K. Wei, W. Shao, H. Ou, and B. Z. Wang, "Efficient WLP-FDTD with complex frequency-shifted PML for super-resolution analysis," *IEEE Antennas Wireless Propagat. Lett*., vol. 16, pp. 1007-1010, 2017.

[8] D. Zhao, Y. Jin, B. Z. Wang, and R. Zang, "Time reversal based broadband synthesis method for arbitrary structured beam-steering arrays," *IEEE Trans. Antennas Propag*., vol. 60, no. 1, pp. 164-173, Jan. 2012.

[9] M. D. Hossain, A. S. Mohan, and M. J. Abedin, "Beamspace time-reversal microwave imaging for breast cancer detection," *IEEE Antennas Wireless Propag. Lett*., vol. 12, pp. 241-244, 2013.

[10] D. Zhao, and M. Zhu, "Generating microwave spatial fields with arbitrary patterns," *IEEE Antennas Wireless Propag. Lett*., vol. 15, pp. 1739-1742, 2016.

[11] W. Fan, Z. Chen, and W. J. R. Hoefer, "Source reconstruction from wideband and band-limited responses by FDTD time reversal and regularized least squares," *IEEE Trans. Microw. Theory Techn*., vol. 65, no. 12, pp. 4785-4793, Dec. 2017.

[12] H. Zhao, Y. Zhang, J. Hu, and Z. Chen, "Hybrid sparse reconstruction-method of moments for diagnosis of wire antenna arrays," *Appl. Comput. Electrom. Society J*., vol. 32, no. 10, pp. 882-887, Oct. 2017.

[13] Y. F. Shu, X. C. Wei, R. Yang, and E. X. Liu, "An iterative approach for EMI source reconstruction based on phaseless and single-plane near-field scanning," *IEEE Trans. Electromagn. Compat.*, vol. 60, no. 4, pp. 937-944, Aug. 2018.

[14] H. Zhao, Y. Zhang, J. Hu, and E. P. Li, "Iteration-free phase retrieval for directive radiators using field amplitudes on two closely-separated observation planes," *IEEE Trans. Electromagn. Compat.*, vol. 58, no. 2, pp. 607-610, Apr. 2016.

[15] A. Taflove and S. C. Hagness, *Computational Electromagnetics: The Finite-Difference Time-Domain Method*. Norwood, MA, USA: Artech House, 2005.

[16] K. Xiao, D. J. Pommerenke, and J. L. Drewniak, "A three-dimensional FDTD subgridding algorithm with separated temporal and spatial interfaces and related stability analysis," *IEEE Trans. Antennas Propag*., vol. 55, no. 7, pp. 1981-1990, July 2007.

[17] C. Chang and C. D. Sarris, "A spatially filtered finite-difference time-domain scheme with controllable stability beyond the CFL limit: Theory and applications," *IEEE Trans. Microw. Theory Techn.*, vol. 61, no. 1, pp. 351-359, Jan. 2013.

[18] X. K. Wei, X. Zhang, N. Diamanti, W. Shao, and C. D. Sarris, "Sub-gridded FDTD modeling of ground penetrating radar scenarios beyond the Courant stability limit," *IEEE Trans. Geosci. Remote Sensing*, vol. 55, no. 12, pp. 7189-7198, Dec. 2017.

[19] S. D. Gedney, "An anisotropic perfectly matched layer-absorbing medium for the truncation of FDTD lattices," *IEEE Trans. Antennas Propag*., vol. 44, no. 12, pp. 1630-1639, Dec. 1996.

[20] D. Cassereau and M. Fink, "Time reversal of ultrasonic fields—Part III: Theory of the closed time-reversal cavity," *IEEE Trans. Ultrasonic, Ferroelectron., Frequency Control*, vol. 39, no. 5, pp. 579-592, Sep. 1992.

Xiao-Kun Wei was born in Tianshui, Gansu Province, China, in 1990. He received the B.S. degree in Electronic Information Science and Technology and the M.Sc. degree in Electronics and Communication Engineering from the University of Electronic Science and Technology of China (UESTC), Chengdu, Sichuan, China, in 2013 and 2015, respectively. Now, he is currently pursuing the Ph.D. degree in Radio Physics at UESTC.

From Sep. 2016 to Aug. 2017, he was an International Visiting Graduate Student with the Department of Electrical and Computer Engineering, University of Toronto, Toronto, ON, Canada. His research interests include unconditionally stable and fast time-domain numerical methods and optimization techniques in electromagnetics.

Wei Shao was born in Chengdu, China, in 1975. He received the B.E. degree in Electrical Engineering from UESTC in 1998, and received M.Sc. and Ph.D. degrees in Radio Physics from UESTC in 2004 and 2006, respectively.

He joined the UESTC in 2007 and is now a Professor there. From 2010 to 2011, he was a Visiting Scholar in the Electromagnetic Communication Laboratory, Pennsylvania State University, State College, PA. From 2012 to 2013, he was a Visiting Scholar in the Department of Electrical and Electronic Engineering, Hong Kong University. His research interests include computational electromagnetics and antenna design.

Xiao Ding received the Ph.D. degree in Radio Physics from UESTC in 2014.

In 2013, he was a Visiting Scholar with the Department of Electrical and Computer Engineering, South Dakota School of Mines and Technology, SD, USA. From June 2016 to June 2017, he was a Visiting Scholar with the Applied Electromagnetics Laboratory, University of Houston, TX, USA. He joined the UESTC in 2014 and he is currently an Associate Professor. His research interests include antenna theory and computational electromagnetics.

Bing-Zhong Wang received the Ph.D. degree in Electrical Engineering from UESTC in 1988.

He joined the UESTC in 1984 where he is currently a Professor. He has been a Visiting Scholar at the University of Wisconsin-Milwaukee, a Research Fellow at the City University of Hong Kong, and a Visiting Professor in the Electromagnetic Communication Laboratory, Pennsylvania State University, State College, PA. His current research interests are in the areas of computational electromagnetics, antenna theory and technique, and electromagnetic compatibility analysis.